

A SIMPLE CHAOTIC FLOW WITH A CONTINUOUSLY ADJUSTABLE ATTRACTOR DIMENSION

BUNCHA MUNMUANGSAEN
*Fabrinet Co., Ltd, Klongluang,
Patumthani, 12120, Thailand
nopnop99@hotmail.com*

JULIEN CLINTON SPROTT
*Department of Physics, University of Wisconsin - Madison,
Madison, WI 53706, USA
sprott@physics.wisc.edu*

WESLEY JOO-CHEN THIO
*Department of Electrical and Computer Engineering, The Ohio State University,
Columbus OH, 43210, USA
wesley.thio@gmail.com
thio.7@osu.edu*

ARTURO BUSCARINO
*Dipartimento di Ingegneria Elettrica Elettronica ed Informatica, Universit degli Studi di Catania,
viale A. Doria 6, 95125 Catania, Italy
arturo.buscarino@dieei.unict.it*

LUIGI FORTUNA
*Dipartimento di Ingegneria Elettrica Elettronica ed Informatica, Universit degli Studi di Catania,
viale A. Doria 6, 95125 Catania, Italy
luigi.fortuna@dieei.unict.it*

Received (to be inserted by publisher)

This paper describes two simple three-dimensional autonomous chaotic flows whose attractor dimensions can be adjusted continuously from 2.0 to 3.0 by a single control parameter. Such a parameter provides a means to explore the route through limit cycles, period-doubling, dissipative chaos, and eventually conservative chaos. With an absolute-value nonlinearity and certain choices of parameters, the systems have a vast and smooth continual transition path from dissipative chaos to conservative chaos. One system is analyzed in detail by means of the largest Lyapunov exponent, Kaplan-Yorke dimension, bifurcations, coexisting attractors, and eigenvalues of the Jacobian matrix. An electronic version of the system and has been constructed and shown to perform in accordance with expectations.

Keywords: Chaos; Dynamical system; Differential equation; Conservative system; Low dimensional chaos.

1. Introduction

The modern chaos era began when the meteorologist Edward Lorenz accidentally discovered sensitive dependence on initial conditions while modelling atmospheric convection on his primitive digital computer, leading to the development of the celebrated Lorenz equations [Lorenz, 1963]. His discovery motivated a search for other simple chaotic systems (e.g. Rössler system [Rössler, 1976], jerk systems [Sprott, 1997], chaotic snap flows [Munmuangsaen & Srisuchinwong, 2011; Sprott, 2010]), chaotic circuits (e.g. Chua's circuit [Fortuna *et al.*, 2009], Lorenz-based chaotic circuit [Blakely *et al.*, 2007]) and applications [Carroll & Pecora, 1991; Cuomo & Oppenheim, 1993; Kiliyas *et al.*, 1995; Kocarev *et al.*, 1992; Srisuchinwong & Munmuangsaen, 2011].

Maximally complex Lorenz and Rössler systems have been studied by Sprott [Sprott, 2007] where complexity is assumed to be given by the Kaplan-Yorke dimension [Kaplan & Yorke, 1979]. He also showed that the Lorenz system can be simplified by using a linear transformation, and its complexity can be optimized by adjusting the control parameters. However, the dimension of the system is still relatively low, i.e., D_{KY} is close to 2.0.

One characteristic of most algebraically simple autonomous chaotic systems is that they produce low-dimensional attractors [Sprott, 1994, 2010]. By contrast, most of the dissipative chaotic equations that can produce high D_{KY} are relatively complicated [Chlouverakis & Sprott, 2004] or require external forcing.

In this paper, we describe two simple three-dimensional autonomous systems whose attractor dimensions (D_{KY}) can be adjusted continuously from 2.0 to 3.0 by a single control parameter. They provide unusual examples of a continuous transition from dissipative chaos to conservative chaos. One of the systems has been studied in detail and implemented electronically. Since it is three-dimensional with a large Kaplan-Yorke dimension, it provides an attractive alternative to the use of hyperchaotic circuits for secure communications [Qi *et al.*, 2008].

2. Dissipative Case with $-bx$ Damping

One simple and elegant example of a conservative system that has been long known and intensively studied is the Nosé-Hoover oscillator [Posh *et al.*, 1986; Hoover, 1995] given by:

$$\begin{aligned}\dot{x} &= y \\ \dot{y} &= yz - x \\ \dot{z} &= a - y^2\end{aligned}\tag{1}$$

where the overdot denotes a time derivative. This system represents a harmonic oscillator in contact with a thermal bath where the nonlinear damping (yz) acts as a thermostat that steers the instantaneous normalized temperature (y^2) to a value given by the single parameter a .

Most initial conditions produce trajectories that lie on invariant tori, but some give chaos, e.g. $(x_0, y_0, z_0) = (0, 5, 0)$. Conservative systems have the rate of volume expansion

$$V^{-1}\left(\frac{dV}{dt}\right) = \text{Tr}J = \frac{\partial \dot{x}}{\partial x} + \frac{\partial \dot{y}}{\partial y} + \frac{\partial \dot{z}}{\partial z} = \lambda_1 + \lambda_2 + \lambda_3 = 0$$

when averaged along the trajectory, where J is the Jacobian matrix and λ_i are the Lyapunov exponents. Although the Nosé-Hoover system has $\text{Tr}J = z$, which is not obviously conservative, numerical calculations indicate that it is [Sprott, 2003], and this result is consistent with the time-reversal invariance of Eq. (1) and symmetry of the solutions. A generalization in which the nonlinear term (y^2) in the \dot{z} equation is replaced with $|y|^\gamma$ has also been studied [Sprott, 2010].

Two simple ways to make the system dissipative are to add a damping term $-bx$ to the \dot{x} equation or to add a damping term $-bz$ to \dot{z} equation. Introducing a damping term $-by$ to the \dot{y} equation merely shifts the trajectory in the z -direction such that $\langle z - b \rangle$ remains zero.

By adding the $-bx$ term, Eq. (1) becomes:

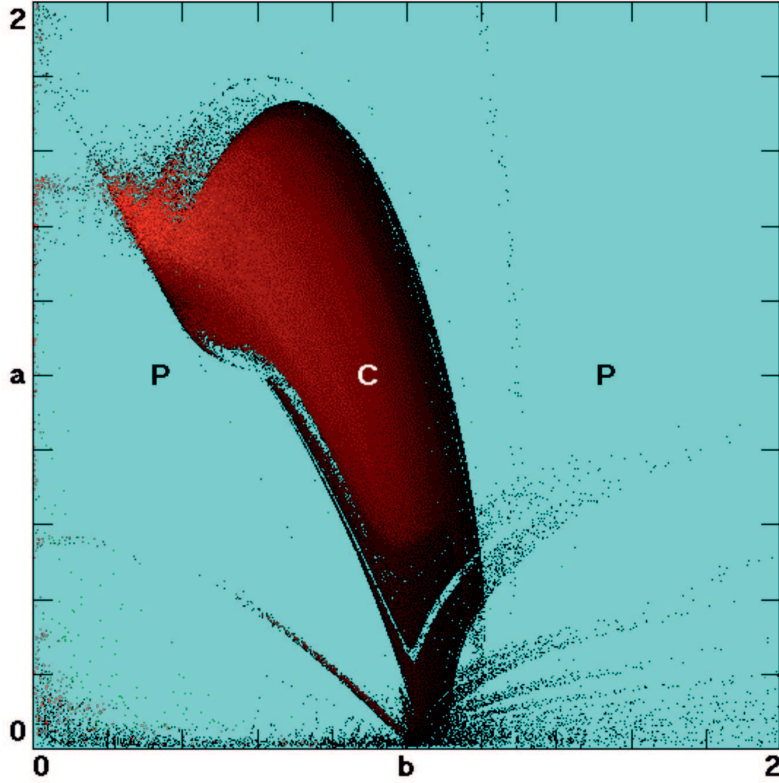


Fig. 1. Dynamic regions in the a - b plane for Eq. (2).

$$\begin{aligned}\dot{x} &= y - bx \\ \dot{y} &= yz - x \\ \dot{z} &= a - y^2\end{aligned}\tag{2}$$

which corresponds physically to a damped harmonic oscillator in contact with a thermal bath. Figure 1 shows the chaotic region in the a - b plane with a continuum red-scale plot indicating the system dimension (D_{KY}) in the range of 2 to 3. Each pixel in the plot uses different initial conditions chosen from a Gaussian distribution with mean zero and variance 1.0. The trajectory was calculated using a fourth-order Runge-Kutta method with adaptive step size and a maximum absolute error of 10^{-6} at each iteration. The criterion used for chaos is that the largest Lyapunov exponent (LLE) must exceed 0.001, and each orbit was followed for a time of $t = 10^5$. Although there are strange attractors for many choices of a and b , there is no continuous path in the plane corresponding to a continuously increasing attractor dimension from 2.0 to 3.0 as the damping parameter b approaches zero.

One way to extend the chaos to lower values of the damping is to replace the y^2 in the \dot{z} equation with a weaker nonlinearity $|y|$,

$$\begin{aligned}\dot{x} &= y - bx \\ \dot{y} &= yz - x \\ \dot{z} &= a - |y|\end{aligned}\tag{3}$$

This modification has the advantage that $|y|$ can be implemented electronically using diodes without the need for an analog multiplier. The chaotic region in the a - b plane of this new system has a vast and smooth continuous path as b gradually decreases to zero as shown in Fig. 2. It happens that $a = 5$ is a particularly good choice because other smaller values have a narrow periodic window (too small to see in the figure) at very low values of b that interrupts the continuous transition from a dissipative chaotic

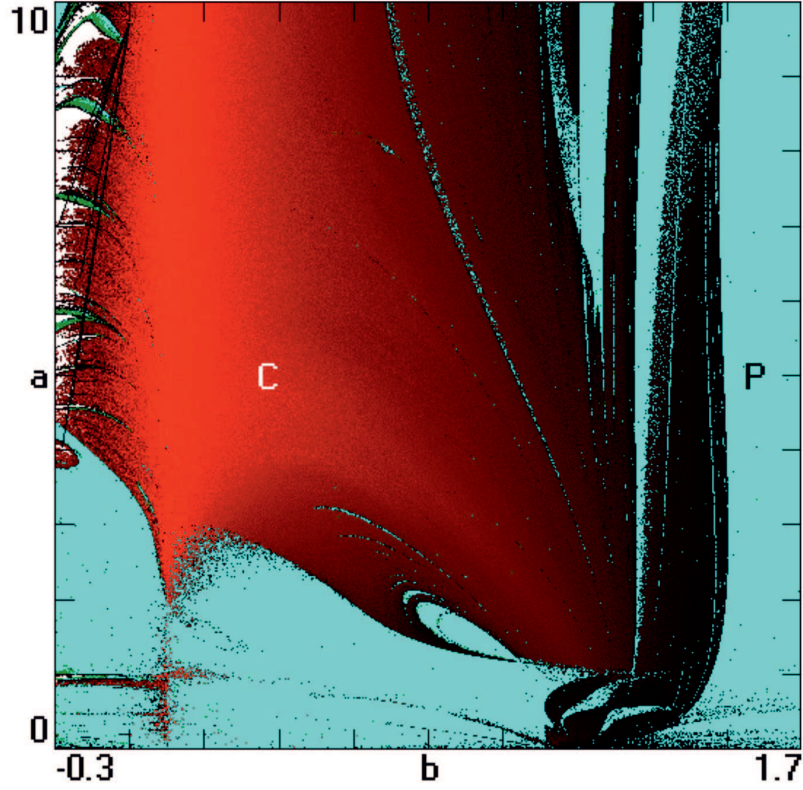


Fig. 2. Dynamic regions in the a - b plane for Eq. (3).

system to a conservative chaotic system. Surprisingly, there are also bounded orbits and chaos for $b < 0$, but these chaotic regions contain numerous periodic and unbounded windows.

Figure 3 shows (from top to bottom) regions of coexisting attractors (where $\langle x \rangle$ is multivalued), the largest Lyapunov exponent (LLE), the Kaplan-Yorke dimension (D_{KY}), and the local maxima of z ($M(z)$) as a function of b for $a = 5$. In the plot of $\langle x \rangle$, many different random initial conditions were used for each value of b , and the mean value of x is plotted for each case. In these plots the parameter b is swept upward without changing the initial condition and plotted in green, and then swept downward and plotted in red to illustrate better the regions where hysteresis and multistability occur.

The system has coexisting limit cycles for $b > 1.5$ that period-double until chaos onsets when b falls to about 1.5, after which a symmetric pair of strange attractors is formed that merge into one large symmetric strange attractor at about $b = 1.42$. The system remains chaotic all the way to $b = 0$ except for some small periodic windows. In the largest of these windows around $b = 1.32$, there is a region of hysteresis where a strange attractor (red) coexists with a limit cycle (green). The maximum $LLE = 0.2086$ occurs at $b \approx 0.64$ where the Kaplan-Yorke dimension is $D_{KY} = 2.4691$. Figure 4 shows trajectories projected onto the x - z plane with coexisting limit cycles for $b = 50$ and $b = 1.8$, two coexisting strange attractors for $b = 1.42$, and a single strange attractor with maximum chaoticity for $b = 0.64$. Interestingly, when the attractors merge, they do so along an entire edge rather than at a single point.

3. Dissipative Case with $-bz$ Damping

Another way to make the system in Eq. (1) dissipative is to add a $-bz$ term to the \dot{z} equation,

$$\begin{aligned} \dot{x} &= y \\ \dot{y} &= yz - x \\ \dot{z} &= a - y^2 - bz \end{aligned} \quad (4)$$

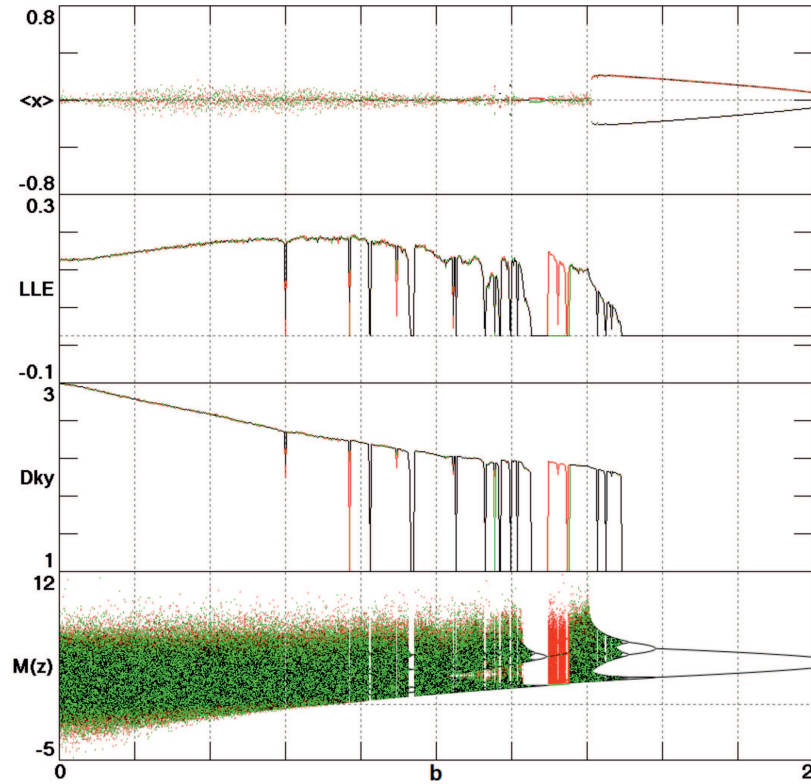


Fig. 3. (From top to bottom) Regions of coexisting attractors ($\langle x \rangle$), the largest Lyapunov exponent (LLE), Kaplan-Yorke dimension (D_{KY}), and local maxima of z ($M(z)$) as a function of b with $a = 5$ for Eq. (3).

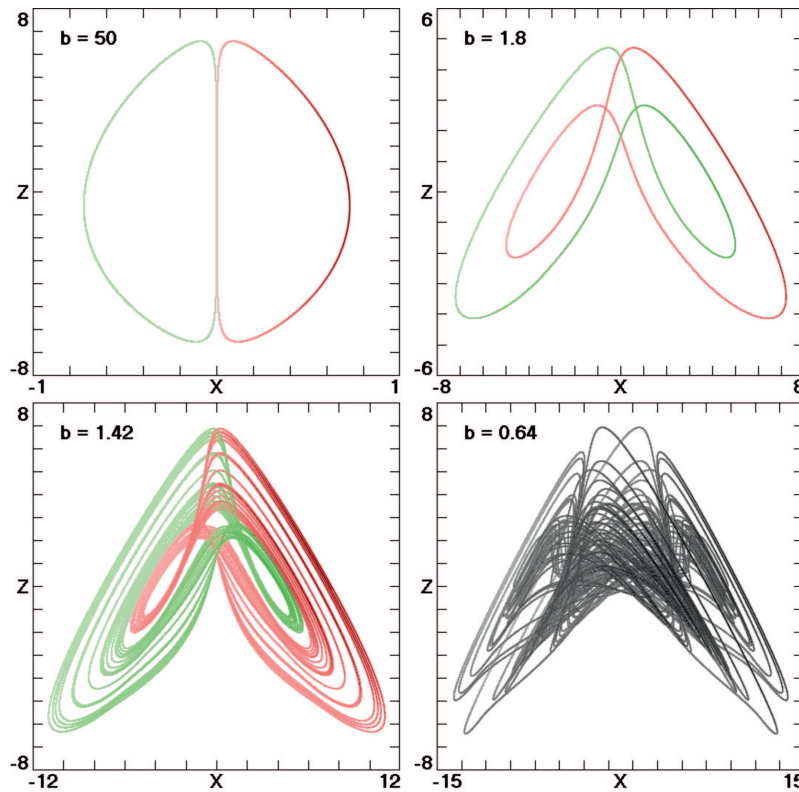


Fig. 4. (a) Trajectories projected onto the x - z plane of limit cycles for $b = 50$, (b) and for $b = 1.8$, (c) two coexisting strange attractors for $b = 1.42$, and (d) a single strange attractor where the maximum chaos occurs at $b = 0.64$ for $a = 5$.

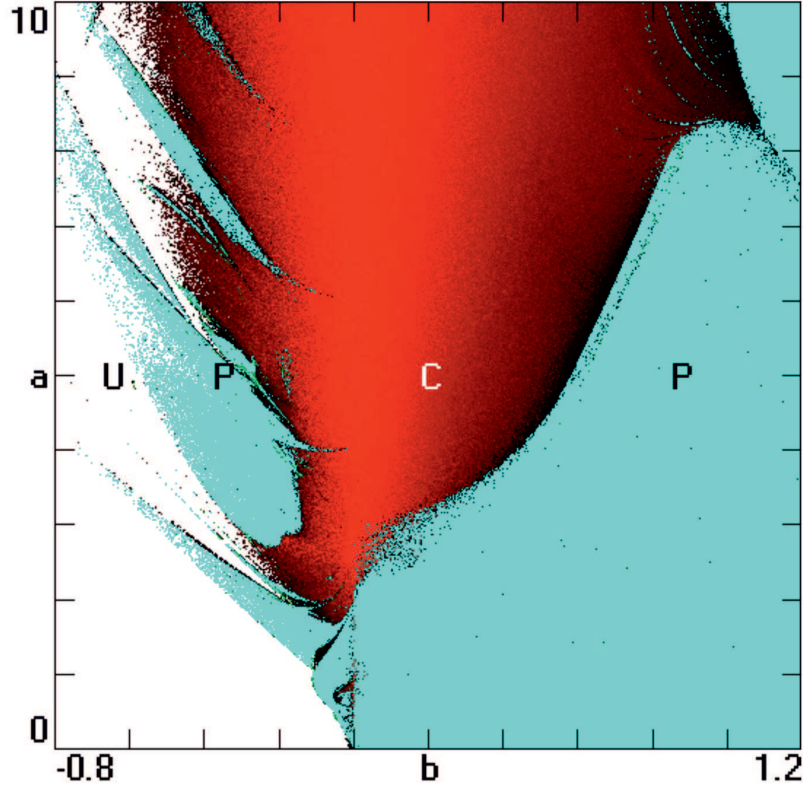


Fig. 5. Dynamic regions in the a - b plane for Eq. (5).

However, the chaotic region in the a - b plane of Eq. (4) is very narrow and mainly occurs for negative b (not shown). A broader and smoother region of chaos occurs if the y^2 nonlinearity in Eq. (4) is replaced with $|y|$,

$$\begin{aligned}\dot{x} &= y \\ \dot{y} &= yz - x \\ \dot{z} &= a - |y| - bz\end{aligned}\tag{5}$$

as shown in Fig. 5. The chaotic region in the a - b plane of this system has no obvious periodic windows as b gradually decreases to zero. The continuum red-scale plot indicates the continuous change of dimension (D_{KY}) in the range of 2 to 3, and a smooth transition occurs for a wide range of a . For $b > 0$, it appears that the attractors are globally attracting except for a set of measure zero corresponding to the infinitely many unstable periodic orbits embedded in the strange attractor.

Equation (5) has a single equilibrium point at $(0, 0, a/b)$ for $b \neq 0$. The linear stability of this equilibrium is determined from the eigenvalues of the Jacobian matrix

$$J = \begin{bmatrix} 0 & 1 & 0 \\ -1 & z & y \\ 0 & -\text{sgn}(y) & -b \end{bmatrix}.\tag{6}$$

When the system is weakly dissipative, the equilibrium has three real eigenvalues of the form m , n , $-p$ (m and p are small but n is large) corresponding to a saddle node of index-2. In the limit $b \rightarrow 0$, one real eigenvalue goes to plus infinity while the remaining ones approach zero, and the equilibrium moves far from the origin. In this range, chaos fully dominates, and the attractor dimension smoothly increases to 3.0 (where the system has no attractors) without any obvious embedded periodic windows, as can be seen

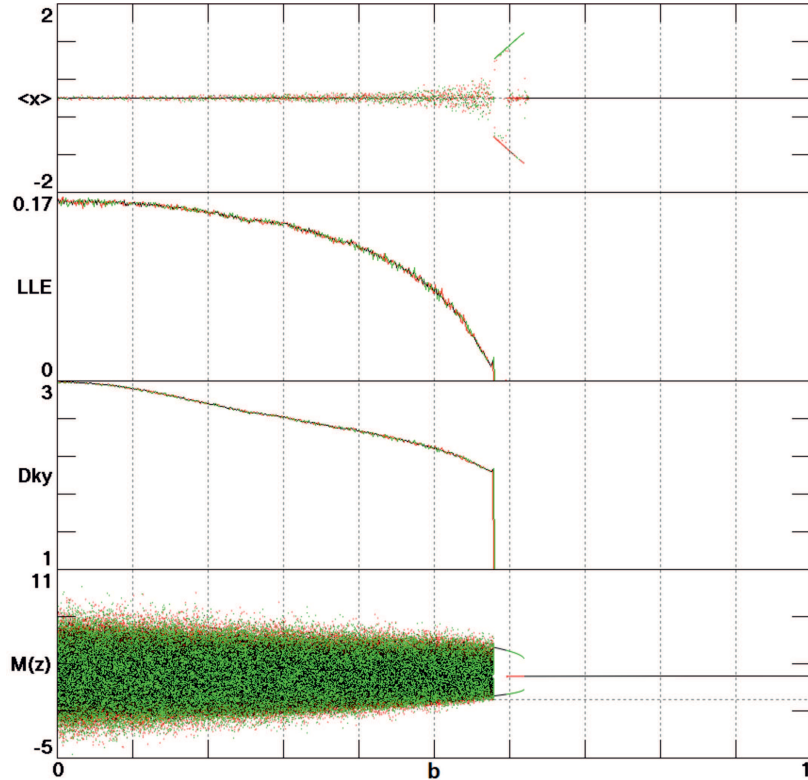


Fig. 6. (From top to bottom) Regions of coexisting attractors ($\langle x \rangle$), the largest Lyapunov exponent (LLE), Kaplan-Yorke dimension (D_{KY}), and local maxima of z ($M(z)$) as a function of b with $a = 5$ for Eq. (5).

from Fig. 6 with $a = 5$. Such a well-behaved trend is rare and is good for studies in which a continuously variable attractor dimension is desired.

When b is very large, there is a single symmetric circular limit cycle near the $z = 0$ plane. As b decreases, a symmetry breaking bifurcation occurs around $b = 0.620$, and a symmetric pair of limit cycles is born. The three attractors as shown in Fig. 7 for $b = 0.6$ coexist until $b \approx 0.596$ where the symmetric one abruptly vanishes. The remaining two limit cycles merge at $b \approx 0.578$, which also marks the onset of chaos with a single symmetric strange attractor. As b decreases from 0.57 to 0, the attractor gradually increases in size and eventually becomes conservative at $b = 0$ where the largest Lyapunov exponent reaches a value of 0.1610.

Figure 8 shows cross sections of the trajectories for Eq. (5) that puncture the $z = 0$ plane for six different values of b with $a = 5$. The multifractal structure becomes more dense as the system dimension increases, and these cross sections confirm the continuously increasing attractor dimension approaching 3.0 as b approaches zero. It is interesting that no quasiperiodic orbits occur for this large value of a , but they do appear when $a \lesssim 2.5$ as illustrated in Fig. 9 where four different values of a are shown. The chaotic sea contains quasiperiodic island chains as is typical for Hamiltonian chaos [Zaslavsky, 2007]. The region of quasiperiodicity grows larger with increasing a until about $a = 2$ where it begins to shrink, apparently vanishing around $a = 2.6$. Thus the system with $a = 5$ and $b = 0$ is apparently ergodic in the sense that a single orbit comes arbitrarily close to every point in the three-dimensional state space [Hoover *et al.*, 2015], and the probability distribution function for the variable x is nearly Gaussian. The ergodicity seems to persist for nonzero values of b , but more exploration of that is needed. For all cases, each orbit was followed for a maximum time of $t = 10^4$. Forty initial conditions were used, spaced uniformly along the vertical midplane. There are two visible horizontal stripes which represent the z -nullclines at $y = \pm a$ in the $z = 0$ plane.

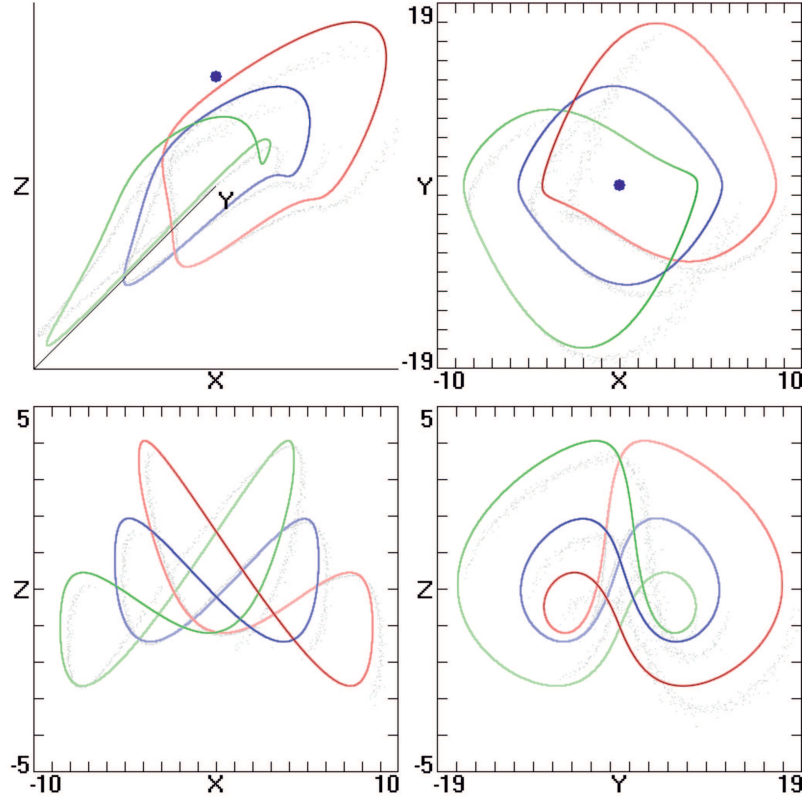


Fig. 7. Three coexisting limit cycles for $a = 5$, $b = 0.6$ from Eq. (5).

4. Experimental Comparisons

In this section, experimental cross sections corresponding to Fig. 8 are presented using an electrical circuit which obeys equation (5). The circuit schematic, realized following standard guidelines [Buscarino *et al.*, 2014], is given in Fig. 10 where each equation in the system is realized by an operational amplifier RC block. Voltages across capacitors are associated with the three state variables. The circuit element values are $C_1 = C_2 = C_3 = 1nF$, $R_1 = R_3 = R_4 = R_5 = R_9 = 100k\Omega$, $R_2 = R_6 = R_7 = 1k\Omega$ and $R_8 = 200k\Omega$. R_{10} is a potentiometer that is used to adjust the value of parameter b . V_b is a fixed bias voltage equal to 1V in order to set the value of parameter a . The diode in the absolute value circuit is 1N4148, and the analog multiplier used to implement the yz nonlinearity is AD633. The operational amplifiers are TL084 integrated circuits powered by 9V supplies. Based on these parameters, the central frequency of operation is 10kHz. The amplitude of the system was rescaled by a factor of 1/10 to avoid saturating the operational amplifiers. The rescaled circuit equations are

$$\begin{aligned} \dot{X} &= \frac{Y}{R_1 C_1} \\ \dot{Y} &= \frac{10YZ}{C_2 R_2} - \frac{X}{C_2 R_3} \\ \dot{Z} &= \frac{V_b}{10C_3 R_8} - \frac{|Y|}{C_3 R_9} - \frac{Z}{C_3 R_{10}} \end{aligned} \quad (7)$$

where $X = \frac{x}{10}$, $Y = \frac{y}{10}$, and $Z = \frac{z}{10}$. The corresponding X-Y, X-Z and Y-Z projections from the oscilloscope are shown in Fig. 11. To obtain the experimental cross sections in these phase planes, the voltages across the three capacitors were acquired using a NI-USB 6255 Data Acquisition Board with a sampling frequency $f_s = 500kHz$ for a total time $T = 8s$. Acquired data was then evaluated to obtain cross sections at $Z = 0$.

Cross sections for different values of the parameter b were obtained by adjusting R_{10} , which implements $b = \frac{100k\Omega}{R_{10}}$. For the range $b = 0.5$ to $b = 0$, R_{10} was adjusted from 200kΩ to 1MΩ and was removed for the case of $b = 0$. Parameter a , which is fixed at $a = 5$, is regulated by setting $R_8 = 200k\Omega$. The experimental

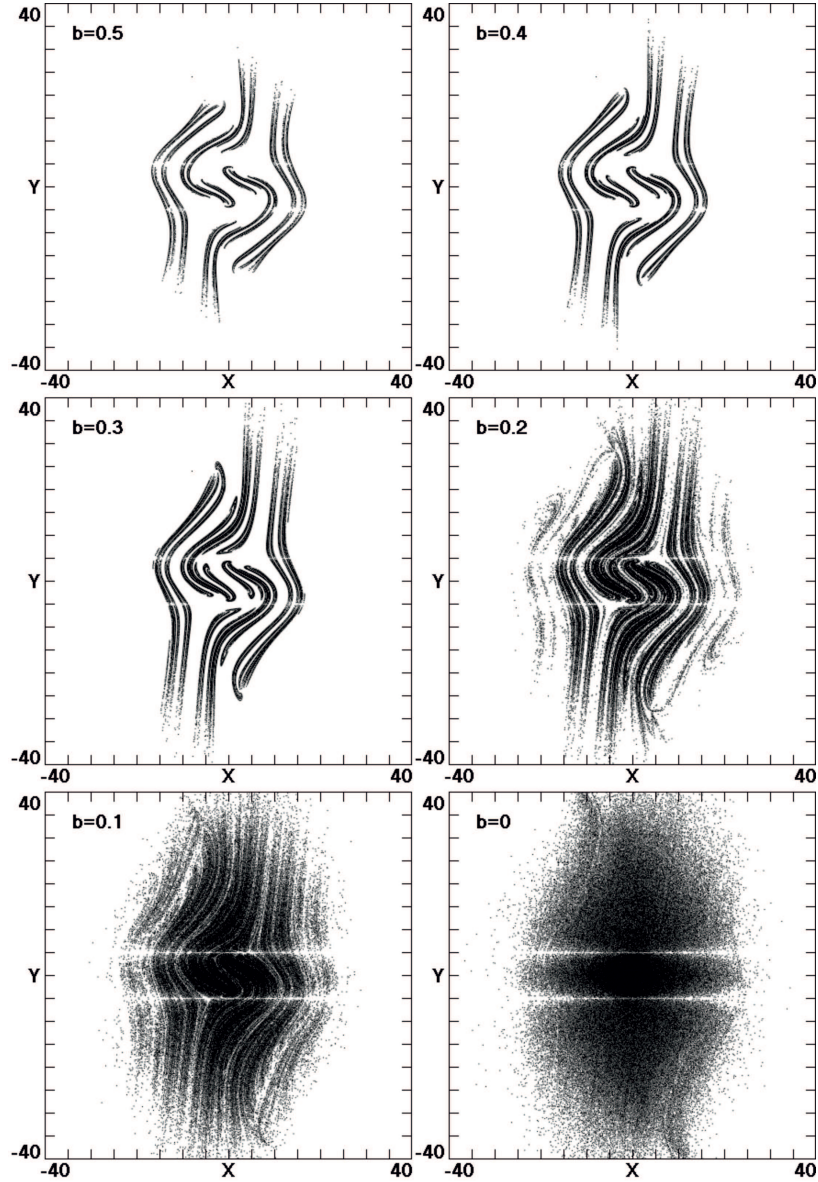


Fig. 8. Cross sections of the trajectories in the $z = 0$ plane for Eq. (5) with $a = 5$.

cross sections are given in Fig. 12. Comparing this experimental figure to the numerical results in Fig. 8 shows the excellent agreement.

Further confirmation of the circuit behavior comes from a comparison between the Kaplan-Yorke dimension D_{KY} and the correlation dimension D_2 calculated from data acquired from the circuit and the same quantities calculated from numerical integration of Eq. (5). The Kaplan-York dimension of the circuit was calculated from $D_{KY} = 2 - \lambda_1 / (\langle 10Z \rangle - b - \lambda_1)$ with the largest Lyapunov exponent λ_1 determined by the method discussed in [Rosenstein *et al.*, 1993]. Figure 13 shows the good agreement and the smooth variation of the dimension over the range 2 to 3 and also suggests that the attractor is multifractal since $D_2 < D_{KY}$.

5. Conclusions

The search for nonlinear models producing chaotic flows with a high degree of complexity often collides with the aim of keeping the model simple. In this paper, two new autonomous chaotic flows have been presented. Despite their mathematical simplicity and the reduced number of parameters, a continuous

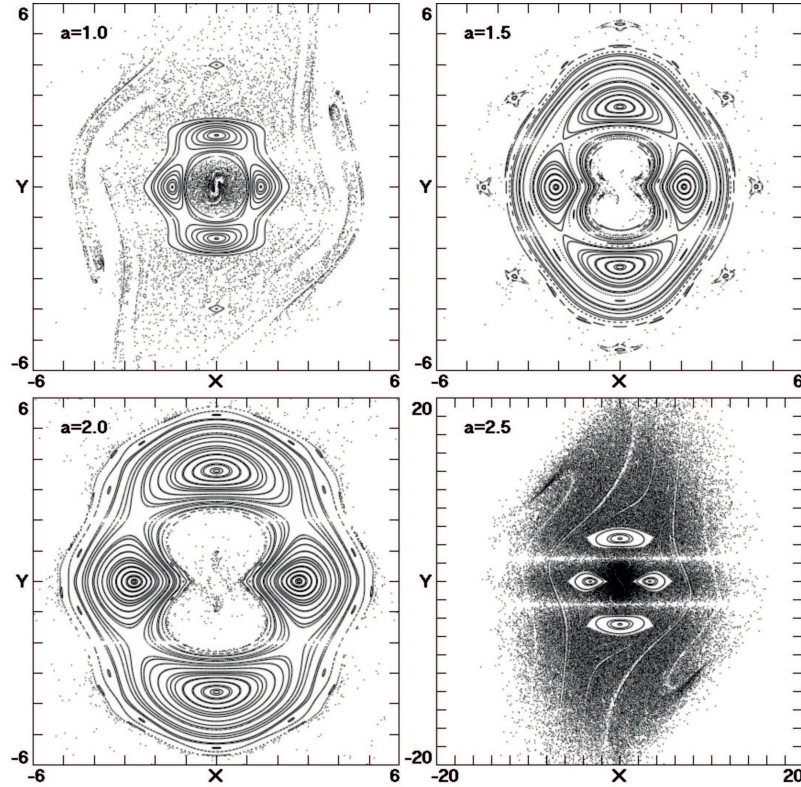


Fig. 9. Cross sections of the trajectories in the $z = 0$ plane for Eq. (5) with $b = 0$.

transition of the attractor dimension from 2.0 to 3.0 has been observed by adjusting a single parameter. When the damping is reduced to zero, the resulting system is ergodic with a nearly Gaussian probability distribution function for x , and a large multifractal dimension. To further illustrate the behavior, one of the models has been implemented electronically and fully characterized. In view of possible applications to secure communications, the proposed circuit has the advantages of using standard off-the-shelf electrical components arranged in a relatively simple manner and of displaying a high level of complexity which can be adjusted by a single resistor.

Acknowledgments

We thank Bill Hoover for his careful reading and insightful comments.

References

- Blakely, J. N., Eskridge, M. B. & Corron, N. J. [2007] "A simple Lorenz circuit and its radio frequency implementation," *Chaos***17**, 023112-1-5.
- Buscarino, A., Fortuna, L., Frasca, M., & Sciuto, G. [2014] *A concise guide to Chaotic Electronic Circuits* (SpringerBriefs in Applied Sciences and Technology).
- Carroll, T. L. & Pecora, L. M. [1991] "Synchronizing chaotic circuits," *IEEE Trans Circuits Syst***38**,453-456.
- Chlouverakis, K. E. & Sprott, J. C. [2004] "A comparison of correlation and Lyapunov dimensions," *Physica D* **200**, 156-164.
- Coumo, K. M. & Oppenheim, A.V. [1993] "Circuit implementation of synchronized chaos with applications to communications," *Phys. Rev. E***71**, 65-68.
- Fortuna, L., Frasca, M. & Xibilia, M. G. [2009] *Chua's Circuit Implementations, Yesterday, Today and Tomorrow*, (World Scientific, Singapore).

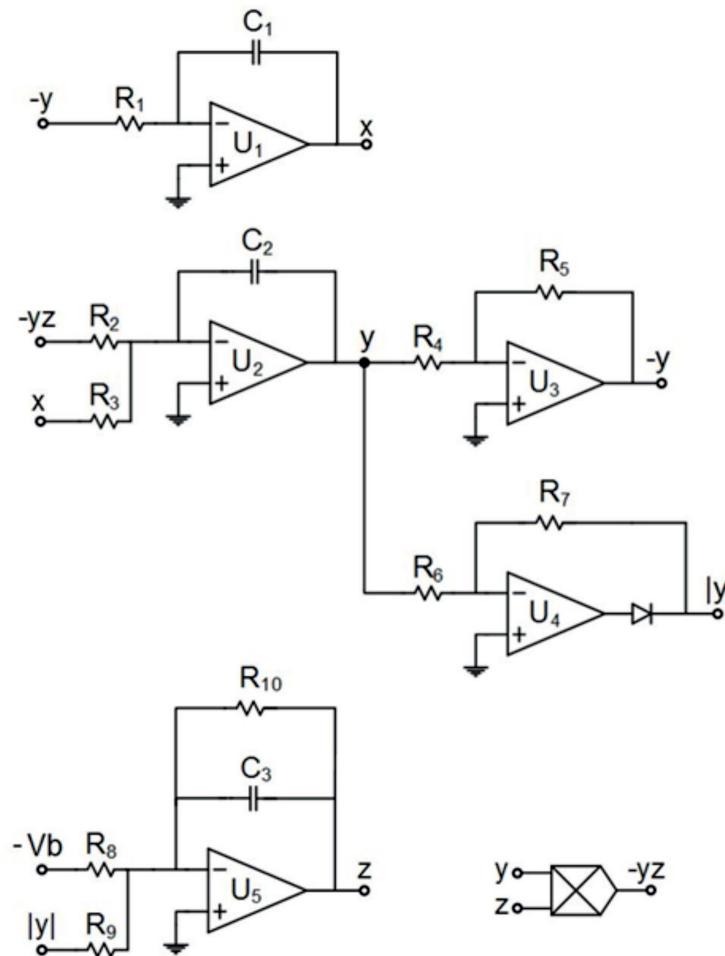


Fig. 10. Electrical circuit schematic.

- Hoover, W. G. [1995] "Remark on some simple chaotic flows," *Phys. Rev. E* **51**, 759–760.
- Hoover, W. G., Sprott, J. C., & Hoover, C. G. [2015] "Ergodicity of a singly-thermostated harmonic oscillator," submitted to *Phys. Rev. E*.
- Kaplan, J. L. & Yorke, J. A. [1979] "Functional differential equations and approximations of fixed points," in *Lecture notes in mathematics* **730**, eds. Peitgen, H.-O. & Walther, H.-O. (Springer, Berlin) pp. 204–227.
- Kilias, T., Kelber, K., Mogel, A., & Schwarz, W. [1995] "Electronic chaos generators: design and applications," *Int J Electron* **79**, 737–753.
- Kocarev, L., Halle, K. S., Eckert, K. & Chua, L. O. [1992] "Experimental demonstration of secure communications via chaotic synchronization," *Int J Bifurcat Chaos* **2**, 709–713.
- Lorenz, E. N. [1963] "Deterministic nonperiodic flow," *J. Atmos. Sci.* **20**, 130–141.
- Munmuangsaen, B. & Srisuchinwong, B. [2011] "Elementary chaotic snap flows," *Chaos Soliton Fract* **44**, 995–1003.
- Posh, H. A., Hoover, W. G. & Vesely, F. J. [1986] "Canonical dynamics of the Nosé oscillator: stability, order, and chaos," *Phys. Rev. A* **33**, 4253–4265.
- Qi, G., van Wyk, M. A., van Wyk, B. J. & Chen, G. [2008] "On a new hyperchaotic system," *Phys. Lett. A* **372**, 124–136.
- Rosenstein, M. T., Collins, J. J., & De Luca, C. J. [1993] "A practical method for calculating largest Lyapunov exponents from small data sets", *Physica D* **65**, 117–134.

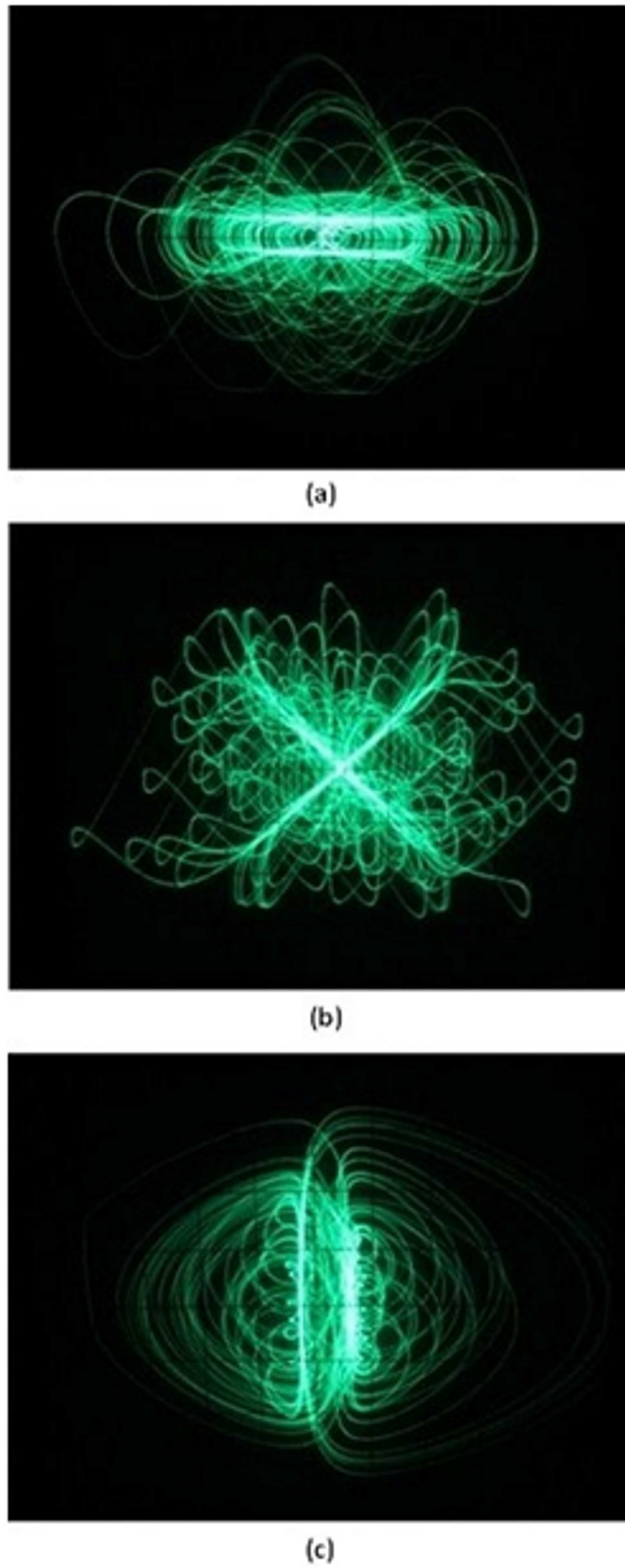


Fig. 11. Oscilloscope traces from the circuit (a) X - Y plane (b) X - Z plane (c) Y - Z plane.

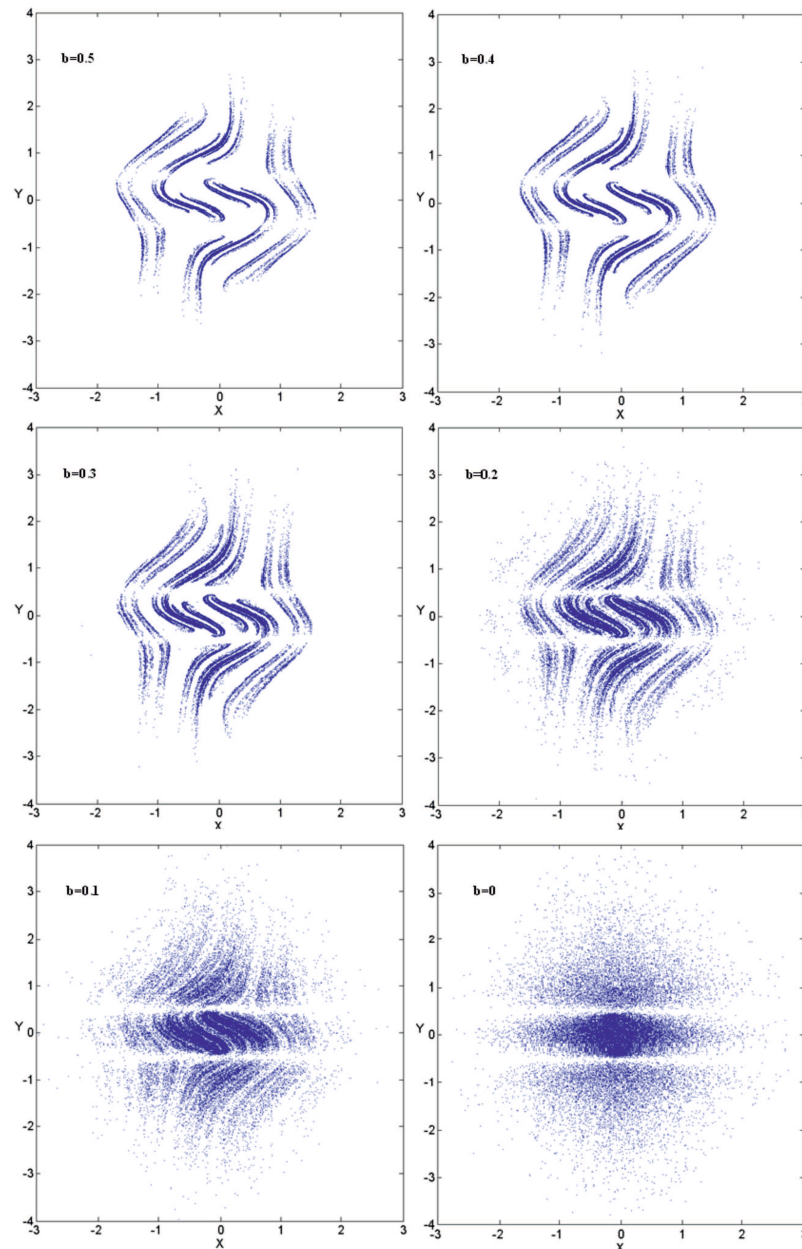


Fig. 12. Experimental cross sections of the trajectories in the $Z = 0$ plane with $a = 5$ ($R_8 = 200k\Omega$).

- Rossler, O. E. [1976] "An equation for continuous chaos," *Phys. Lett.* **A57**, 397–398.
- Sprott, J. C. [1994] "Some simple chaotic flows," *Phys. Rev.* **E50**, R647–650.
- Sprott, J. C. [1997] "Some simple chaotic jerk functions," *Am. J. Phys.* **65**, 537–543.
- Sprott, J. C. [2003] *Chaos and Time-Series Analysis* (Oxford University Press, Oxford).
- Sprott, J. C. [2007] "Maximally complex simple attractors," *Chaos* **17**, 033124-1–6.
- Sprott, J. C. [2010] *Elegant Chaos: Algebraically Simple Chaotic Flows*, (World Scientific, Singapore).
- Srisuchinwong, B. & Munmuangsaen, B. [2011] "A highly chaotic attractor for a dual-channel single-attractor, private communication system," in *Chaos Theory: Modeling, Simulation and Applications*, eds. Skiadas, C. H., Dimotikalis I., & Skiadas, C. (World Scientific, Singapore) pp. 399–405.
- Zaslavsky, G. M. [2007] *The Physics of Chaos in Hamiltonian Systems*, (World Scientific, Singapore).

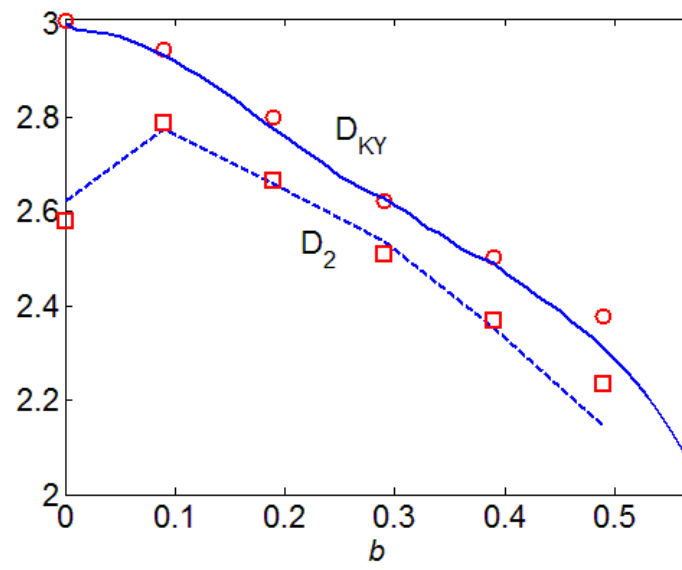


Fig. 13. Kaplan-Yorke and correlation dimensions evaluated for the model (blue lines) and from experimental data acquired from the circuit (red markers: D_{KY} circles, D_2 squares).